International Journal of Non-Linear Mechanics 149 (2023) 104329

Contents lists available at ScienceDirect

International Journal of Non-Linear Mechanics

journal homepage: www.elsevier.com/locate/nlm

On the elastic snapping of structural elements

L.N. Virgin

Department of Mechanical Engineering and Materials Science, Duke University, Durham, NC 27708-0300, USA

ARTICLE INFO

This article is dedicated to the memory of Ilinca Stanciulescu. We had many happy discussions on the nature of snap-through buckling. She is sorely missed.

Keywords:
Snap-through buckling
3D-printing
Reversibility

ABSTRACT

A bistable structural component possesses more than one stable equilibrium configuration. In terms of the strain energy stored in bending, this can be thought of as a system with not only an initial equilibrium configuration represented by an isolated minimum, but also a remote minimum that might be accessed given a sufficient disturbance. Whether the system is able to stay in this new position, or revert back to the initial state when the disturbance is removed is an important practical issue. This distinction is largely determined by geometry. Continuous elastic structures of the type produced using a 3D-printer are necessarily of relatively high-order in a dimensional sense, and most previous studies have used nonlinear finite element analysis to determine parameter sensitivity. However, there is a role to be played by discrete low-order models in which the same type of essential qualitative behavior can be captured, but where the parameter dependency (in this case whether a system stays in its inverted, snapped, configuration, or not) can be assessed more directly than numerical simulation. This short note develops a discrete model specifically designed to address this issue, and presents the outcomes of some tests on 3D-printed elements.

1. Introduction

There has been considerable recent interest in reconfigurable structural forms, often based on a lattice arrangement, that can exhibit snap-through buckling [1,2]. Conventionally, most forms of buckling have been viewed as undesirable, especially when it leads to plastic deformation, or stress-induced brittle failure. However, there are also situations in which structural (elastic) instability can be exploited, and additive manufacturing has provided a versatile and powerful platform for experimentation [3]. One such example is energy trapping [4–6], in which a flexible structural component or lattice is specifically configured such that when compressed it exhibits controlled trapping of elastic energy. That is, the system possesses a highly deformed (higher-energy) stable state that is recoverable, and thus presents intriguing possibilities for architectured and phase-changing materials [7].

Much of the recent impetus in this area has included developments within the scope of micro-electrical mechanical systems (MEMS) and metamaterials, in which specific geometry is exploited to influence features including bi-stability. Applications are myriad, for example, switches and actuators [8,9], soft robotics [10], and locomotion [11], can all benefit from a component designed to suddenly change its topology. Others applications of such structures include impact and energy absorption [4,12–17], origami [18], energy harvesting [19–22], and waveguides [23–25]. 3D-printing is very well suited to producing framework-lattice-type structures, and to relatively high levels of geometric precision [3,26–28].

On the analysis side, the majority of research has involved finite element methods (FEM), numerical simulation [4], together with some large-deflection analysis [29,30]. Often, the snap-through is observed from the lateral loading of a buckled beam or arch [31,32]. Typically this loading is compressive, and assuming the structure is not attached to the loading device, the system will become detached if the load direction is reversed (effectively tensile pulling is not supported). This directly leads to the question: when a load or disturbance is removed, does the structure remain in the 'remote', or closed, equilibrium, or move back to its original, or open, shape. Determining this distinction is the motivation for the current study.

Snap-through is a classic limit-point buckling phenomenon in which the stiffness of a structure under load drops to zero and precipitates a sudden dynamic jump to a remote stable equilibrium configuration [33,34]. On the removal of the load the structure may snap-back or not, and hysteresis is quite typical in this elastic, highly nonlinear situation. In related research, certain specific structural arrangements have been developed to exhibit zero [35], and even negative Poisson's ratio [36–38]. Structural components may snap even under tension [39,40]. Lattice, honeycomb-like structures are especially versatile [41–46] in this regard, and may be activated by temperature changes.

Some prior research has determined the geometric parameter regimes and their influence on bistable behavior of shallow elastic arches [5], and bistable behavior is sometimes precipitated by fluctuations in the thermal environment [47], and in higher-order systems the pathways between stable equilibria can be very complicated indeed [48,49]. Other kinds of buckling have also been explored, including column (Euler-type) buckling [2,6,50,51], but it is worth

E-mail address: l.virgin@duke.edu.

https://doi.org/10.1016/j.ijnonlinmec.2022.104329
Received 16 June 2022; Received in revised form 21 November 2022; Accepted 2 December 2022
Available online 7 December 2022

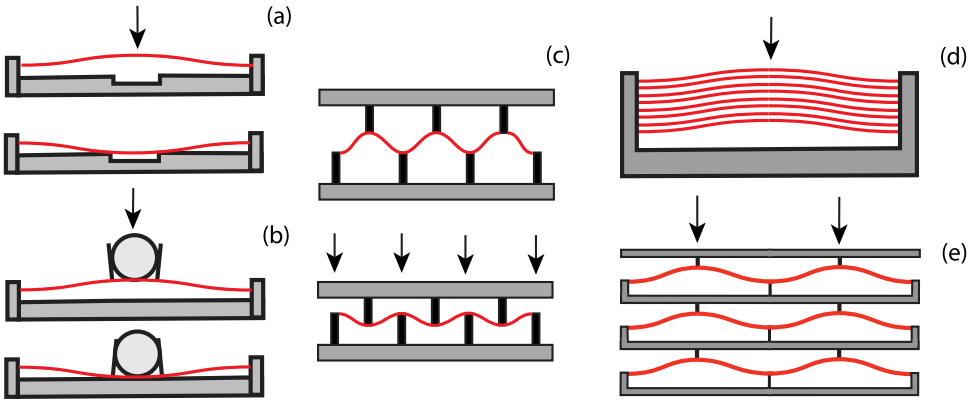

Fig. 1. Some examples of bistable structural arrangements. (a) valve, (b) gripper, (c) snapping elements in parallel, (d) snapping elements in series, (e) snapping lattice. More examples of the 3D-printed lattices can be found in [1,3,30], and the Appendix.

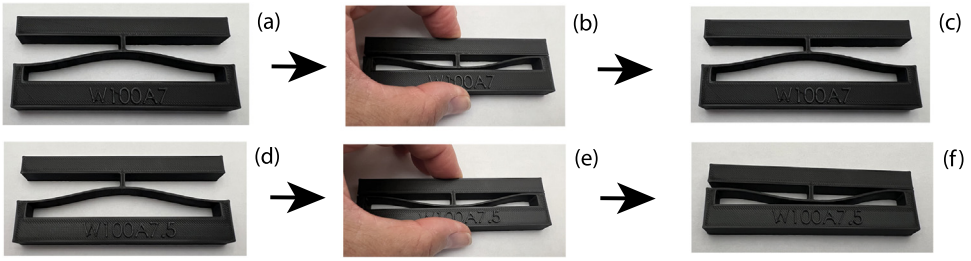

Fig. 2. Two 3D-printed elements that snap. (a)–(c) loading and unloading, (d)–(f) loading and unloading for a slightly deeper curved component.

mentioning that in 3D-printing the initial shape is essentially stress-free (as opposed to a shape that is elastically deformed into an initial shape).

2. Specific motivation

This paper presents a simple discrete model specifically designed to shed light on the conditions under which an arch-like structural component may exhibit bistable behavior. The emphasis is on a single-degree-of-freedom (SDOF) analysis and what it tells us about analogous continuous elastic systems of the type easily produced using 3D-printing. The use of simple discrete models allows an appreciable connection to system parameters [52,53].

Fig. 1 shows a few schematic examples of shallow curved elements that are liable to snap-through, and perhaps remain in a post-buckled configuration.

The specific type of behavior we wish to qualitatively address can be seen in Fig. 2. Here, we note the sequence when two structural elements are subject to compression (and release). In parts (a)–(c), the structure snaps-back to its original configuration on removal of the compression. This contrasts with parts (d)–(f) in which the structure remains in its snapped configuration. The geometric difference between these two is very small, with the structure in the lower panels having a slightly higher rise (all other things being held equal).

3. Qualitative analysis

The essential snap-through behavior of laterally-loaded curved continuous structural components can be captured using a discrete model. A conventional approach might involve a finite element analysis, or some kind of large deflection (elastica) analysis [5], but there is some advantage in developing a relatively simple (single-degree-of-freedom) discrete model that can be analyzed to provide closed-form relations between representative system parameters and snap-through behavior. The approach used here is in the same spirit as that adopted in [52,53].

Consider the model shown schematically in Fig. 3. Part (a) shows two rigid links of length L, connected to each other via a hinge, and also to lateral and axial springs of coefficient c and k respectively. The generalized coordinate θ is measured from the initial angle α. The arch model is constrained to deflect symmetrically, and although a continuous arch typically exhibits some asymmetry (a second mode influence that will be discussed later) especially close to snap-through buckling, the specific form of the 3D-printed elements under consideration here, especially when incorporated within a lattice configuration, result in symmetric 'free' equilibrium configurations. The angle α describes the initial unloaded equilibrium shape, in which the springs are in their natural stress-free condition. The 3D-printed structures are essentially stress-free (as opposed to being deformed from an initially flat beam, for example). Part (b) shows the link model in a loaded/deflected state in which symmetry ensures a vertical deflection Δ_1 under the load P, and a corresponding horizontal deflection Δ_2, with

$$\begin{aligned} \Delta_1 &= L\left[\sin\alpha - \sin(\alpha-\theta)\right] \\ \Delta_2 &= L\left[\cos(\alpha-\theta) - \cos\alpha\right]. \end{aligned} \tag{1}$$

We can write the potential energy V of this system in terms of the strain energy associated with lateral deflection $U_c(\Delta_1)$, axial deflection $U_k(\Delta_2)$, and the work done by the load $W_p(\Delta_1)$:

$$\begin{aligned} V = (1/2)cL^2\left[\sin\alpha - \sin(\alpha-\theta)\right]^2 + kL^2\left[\cos(\alpha-\theta) - \cos\alpha\right]^2 \\ -PL\left[\sin\alpha - \sin(\alpha-\theta)\right] \end{aligned} \tag{2}$$

The behavior of the arch depends on the parameters P, c, k, and α. In reference to the 3D-printed models in the previous section we make the following compelling analogy. We consider the load P as the control parameter, associated with pushing down on the cell or lattice, i.e., via an imposed displacement. The spring c takes on the role of the lateral stiffness of the curved elements, incorporating the beam thickness, length, cross-sectional properties, and the material used. The spring k takes on the role of a little lack of axial rigidity in the models, i.e., there is some flexibility in the supports, and possibly some axial extensibility. It seems plausible that $k \gg c$ for the geometries printed (see Fig. 2).

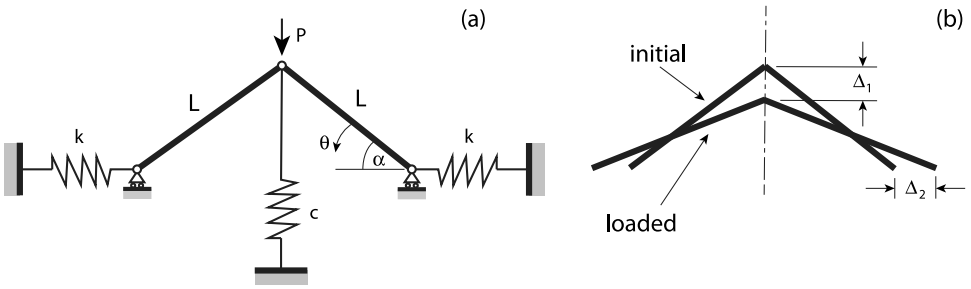

Fig. 3. Schematics of the arch model. (a) the geometry and springs, (b) the initial and loaded/deflected shape.

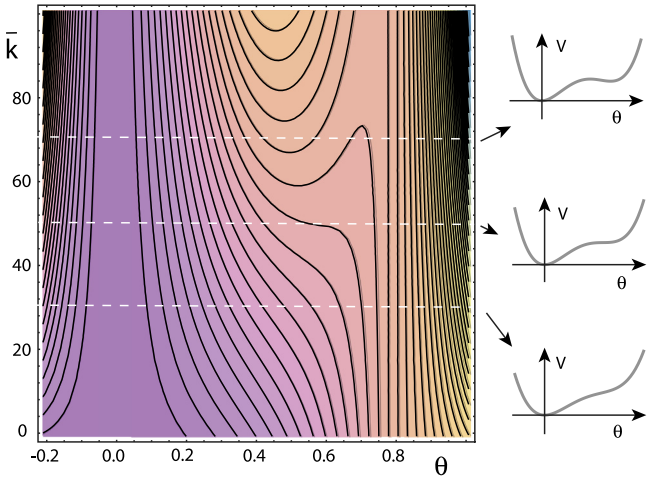

Fig. 4. Contours of potential energy as a function of the angle θ, for the unloaded structure ($P = 0$), i.e., strain energy, and different values of the spring ratio $\bar{k}$, with fixed $\alpha = \pi/8$.

And α represents the rise of the arch, and associated with the initial height/span ratio.

The potential energy of the system possesses a minimum in the unloaded state (at $\theta = 0$). Depending on the ratio of the spring stiffnesses and the rise, the model can also possess a deflected free equilibrium configuration associated with a remote minimum, or not. This is typically associated with configurations in which the arch is somewhat inverted. Contours of potential energy, as a function of the spring ratio $\bar{k} = 2k/c$, are shown in Fig. 4. The transition between a geometry with a single (unique) equilibrium configuration and one exhibiting three equilibria (one of which is typically unstable) corresponds to a point of inflection in the potential energy (the middle inset in Fig. 4). That is, for small values of $\bar{k}$ (a stronger axial than lateral spring stiffness) the unloaded model can only maintain its initial configuration in the absence of any external load or constraint. The key issue is then access to that remote equilibrium given either a (not necessarily small) dynamic disturbance, or, as the case of interest here, a uni-directional force. That is, a system limited to positive values of the load P only, that determines energy trapping.

We consider the behavior of the model under the action of the load. The condition for equilibrium is $dV/d\theta = 0$, from which we obtain

$$\bar{p} = \sin\alpha - \sin(\alpha - \theta) + \bar{k}\,[\cos(\alpha - \theta) - \cos\alpha]\tan(\alpha - \theta) \tag{3}$$

where $\bar{p} = P/(cL)$ and $\bar{k} = 2k/c$.

We start by fixing the model in its initial configuration, characterized by α, and consider the force–deflection behavior described by Eq. (3) for a few sample parameter values. Fig. 5(a) shows typical responses for $\alpha = \pi/8$, with the initial shape labeled point 1. Setting $\bar{k} = 70$ we observe an initially linear response before a softening effect as the load $\bar{p}$ is increased. At $(\bar{p}, \theta) = (0.98, 0.186)$ a horizontal tangency is encountered (point 2), the conventional stiffness has dropped to zero, and a sudden snap would cause the system to undergo a fast inversion to point 5, where $(\bar{p}, \theta) = (0.98, 0.802)$, *under a force-control loading*, for example, if the load was due to the application of a free-weight was added.

However, under displacement-controlled loading, the full nonlinear path is followed beyond the horizontal tangency, including where the force becomes negative (the force is pulling on the arch to keep in contact). Depending on the way the loading is applied, the system may lose contact from position 3 to position 4, for example if the structure is free to move (or snap) away from the load.

Configurations in the vicinity of point 5 correspond to some inversion in the shape (buckled down). The interesting behavior occurs during *unloading*. If the load is gradually reduced the system moves to point 4, $(\bar{p}, \theta) = (0, 0.693)$, where it remains: at $\bar{p} = 0$ this is a location of 'free' equilibrium, with positive stiffness. A further loading into negative values (pulling) is needed to cause the system to fully unload. For $\bar{k} = 30$, the system would also experience a snap, albeit more moderate, under dead loading. However, for this case, there is no remote equilibrium, and even though there might be a certain amount of hysteresis (under dead loading), on unloading the force does *not* become negative and hence the system has no choice but to return (eventually) to its original state.

As just illustrated, whether the system stays inverted, or not, depends on whether the force–deflection curve passes back through zero force, and thus the two examples just given (with $\bar{k} = 30$ and 70) span this condition. In the 3D-printed specimens mentioned earlier, the propensity to snap when a structure is pushed together and its propensity to snap-back once the squashing is removed in thus explained. We can determine the condition of where the zero-crossing occurs analytically, i.e., where the equilibrium curve transitions from one root to three roots. For example, $\alpha = \pi/8$, and $\bar{k} \approx 50$, is close to this condition, and occurs at $\theta \approx 0.59$. Any spring stiffness ratio greater than this value leads to sticking behavior, for this value of the initial 'rise'.

In a similar vein, suppose we fix the stiffness ratio at $\bar{k} = 50$ and vary the initial angle α. Fig. 5(b) shows the behavior. In this case the system, characterized by a higher initial angle ($\alpha = \pi/7$), results in a persistent snapped-through shape, whereas a lower initial angle ($\alpha = \pi/9$) does not. This is consistent with the behavior shown in Fig. 2. We also notice that the straight configuration ($\theta = \alpha$) does not play an important role. Furthermore, if $\bar{k} = 0$, we obtain sinusoidal behavior which is essentially linear for small deflections. If $\bar{k} \to \infty$, or $c = 0$, we obtain a system that exhibits an unstable equilibrium configuration when it is straight, i.e., $\theta = \alpha$, and essentially an equal force to cause snapping in either direction symmetrically.

Fig. 6 shows where the force–deflection response passes through zero as a function of the system parameters. Part (a) shows the effect of changing the spring stiffness ratio for a fixed initial angle $\alpha = \pi/8$. We observe the case $\bar{k} = 50$ does not quite meet the zero force condition. Similarly, in part (b) the fixed spring stiffness ratio ($\bar{k} = 50$) does not quite cross the zero-force axis when $\alpha = \pi/8$.

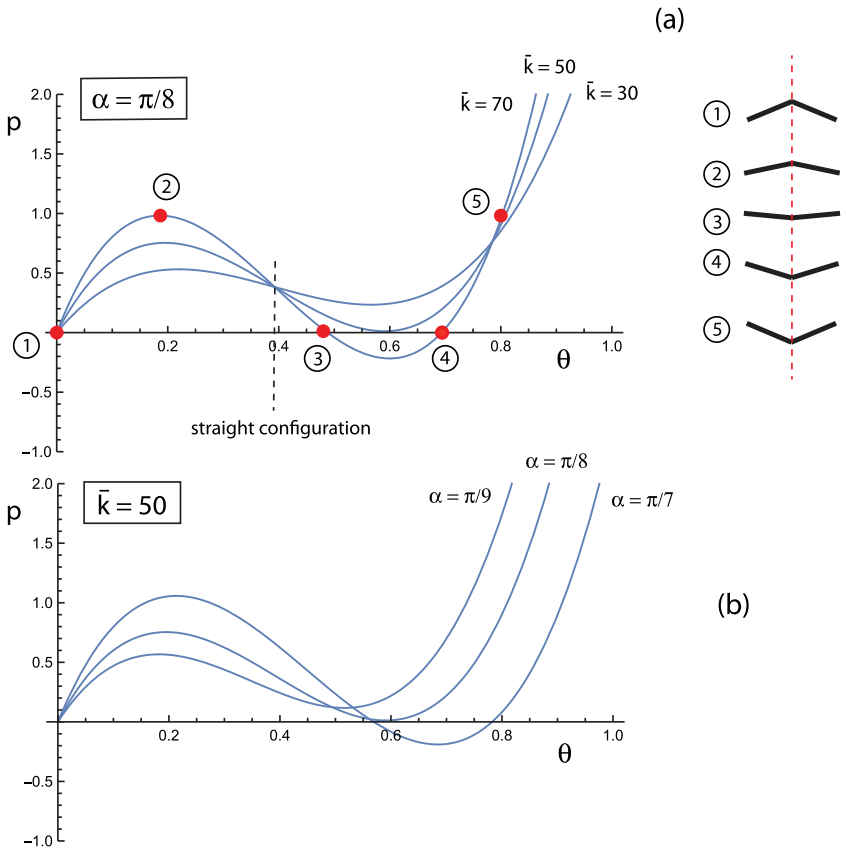

Fig. 5. Force–deflection behavior. (a) $\alpha = \pi/8$, varying $\bar{k}$, (b) $\bar{k} = 50$, varying α.

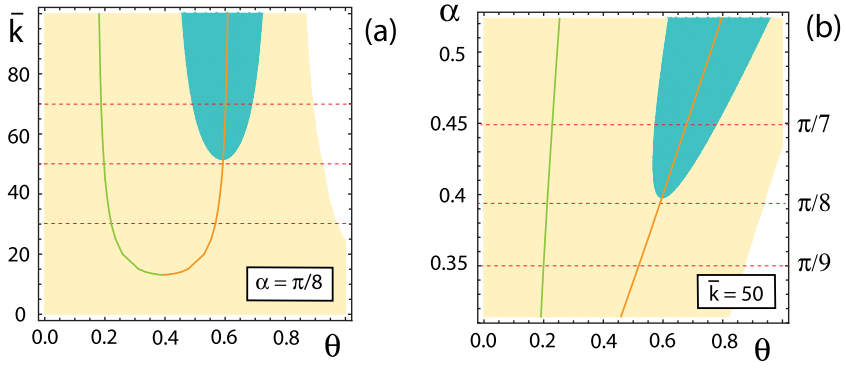

Fig. 6. A summary of the parameters allowing a persistent snapped configuration on removal of the load. (a) $\alpha = \pi/8$, varying $\bar{k}$, (b) $\bar{k} = 50$, varying α. The red-dashed lines correspond to the representative cases described earlier. The green and orange lines correspond to turning points in the load–deflection characteristics. (For interpretation of the references to color in this figure legend, the reader is referred to the web version of this article.)

The turquoise regions correspond to parameter values that possess stable (remote) equilibria indicating the model staying in a partially inverted shape on removal of the load. Also superimposed in this plot are the loci of turning points in the force–deflection relation, with the green lines representing the maximum load and the green lines representing the minimum load. These curves were obtained by solving the equation corresponding to setting the second derivative of potential energy equal to zero. For values of $\bar{k}$ and α outside of these loci, the force–deflection response is monotonic (single-valued) in parts (a) and (b) respectively.

Finally, we can plot the critical condition in parameter space, as shown in Fig. 7. Here the light yellow shading again corresponds to parameter combinations that *do not* possess a remote stable equilibrium. Within the tolerance limits of the root-finding algorithm in Mathematica we obtain more accurate values on the critical boundary: $\alpha = \pi/7.92$ when $\bar{k} = 50$, and $\bar{k} = 51.04$ when $\alpha = \pi/8$. Fig. 7 confirms the intuitive expectation that the model is more likely to stay in a snapped-through position if the initial angle is relatively large, and if the axial springs are somewhat stiffer than the lateral springs, and one can imagine how the critical boundary might be used in a design context.

Although the generalized coordinate used in the model to describe the deflected shape was the angular deviation from the initial configuration, we can also view the response in terms of the vertical

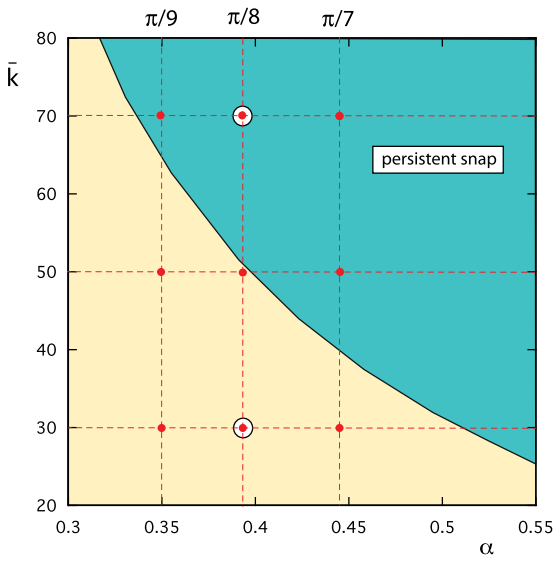

Fig. 7. The regions of parameter space corresponding to a persistence of a snapped-through shape.

deflection (since this is what the experimental data would typically correspond to): $x \equiv \Delta_1$. We note that for the parameters chosen there is very little numerical difference between x/L and θ. Fig. 8 shows two representative examples of force–deflection behavior, one that returns to the initial shapes on removal of the load (part a), and one that stays inverted (part b).

The red and blue arrows represent loading and subsequent unloading, respectively. It is important to recall that this sequence of events corresponds to a displacement-controlled loading device. The stiffness of the remote state (indicated by the red square) reflects the degree of stability in this position.

4. Experimental data

Although the main focus of this paper has been on the qualitative behavior of the simple discrete model, some experimental data, generated from some axial loading of elements, shows the broad relation between the persistency of snap-through with geometry. Consider a typical component, or element, shown in Fig. 9. It consists of two relatively rigid bars that are connected via a thin arch-like element. The span of the arch is 100 mm with a nominal thickness of 1.25 mm. The 'rise' of the arch is the variable that is subject to systematic change: from 5.25 mm to 7.5 mm in 0.25 mm increments. These values were chosen in order to span the geometry between elements that both snapped-back and stayed snapped. These elements were 3D-printed using a Startsys printer with ABS thermoplastic. Part (c) shows a typical element in the testing machine (Lloyds Instruments LRX Plus with a 100 N load cell).

Fig. 10 shows the outcome of the vertical load versus vertical displacement for the ten elements. The testing machine used a prescribed rate of descent (10 mm/minute) to produce the data shown in part (a). The machine moved down until the ends of each element met, after which the direction of loading was reversed. It is important to note that the loading cell is not attached to the element, such that the force only 'pushes' on the element — it cannot 'pull'. Thus, a zero load reading can be associated with a loss of contact.

In each case there was an initial linear response, sometimes followed by a sudden snapping event, marked asymmetry, contact on one side and then fully closing. After the ends of the element are forced together the load rapidly increases. On subsequent unloading the elements either retraced their path back to their original 'open' shape, or stayed in the 'closed' position. The transition between the geometry that snapped-back (open) and stay snapped together (closed) occurs for the element with a rise in the vicinity of 6.5 mm. Part (b) of this figure shows the maximum and minimum loads as a function of the rise. For example, for the most shallow arch (5.25 mm) the maximum load reaches approximately 8 N, and then declines to about 1 N before rapidly rising as the element closes shut. However, as the direction of loading is reversed, the arch retraces its path and opens back onto its original shape. In general, the minimum load occurs at zero for the rise of 6.5 mm and greater, indicating that the elements will stay closed and not remain in contact with the load cell as the loading device moves back up (shaded light yellow). Also, as an example, the element with a rise of 7.5 mm reaches a maximum load of about 13 N before losing contact for a while, until the ends contact. In this case the elements remains in its closed configuration when the loading direction is reversed. The broad regimes of rise that correspond to bi-stability are indicated by the turquoise-shaded region. Thus, we can view Fig. 10(b) as being analogous to a horizontal traverse through Fig. 7, i.e., a varying the rise (initial angle, α) with all other parameters held constant. The light gray shading in this figure indicates a small transition range of geometries for which subtle effects can influence whether an element stays snapped together or not. This will be discussed later.

However, this overall behavior is by no means simple, and in order to focus on the dichotomy surrounding bi-stability behavior we scrutinize two specific cases in more detail: 5.5 mm and 7 mm. These elements are highlighted in blue and red respectively, and replotted in Fig. 11. We start by considering a relatively shallow arch with a rise of 5.5 mm. Under slow loading conditions the (black) data shows a gradually softening stiffness with a maximum load of about 8 N (point A). Very soon after there is a small jump in the response as the arch suddenly tilts to one side (point B). This tilted behavior causes one side to contact (point C) and the deformation proceeds under a reducing load until a minimum is reached (point D). Subsequent deformation then causes both sides to contact and the load rapidly increases (point

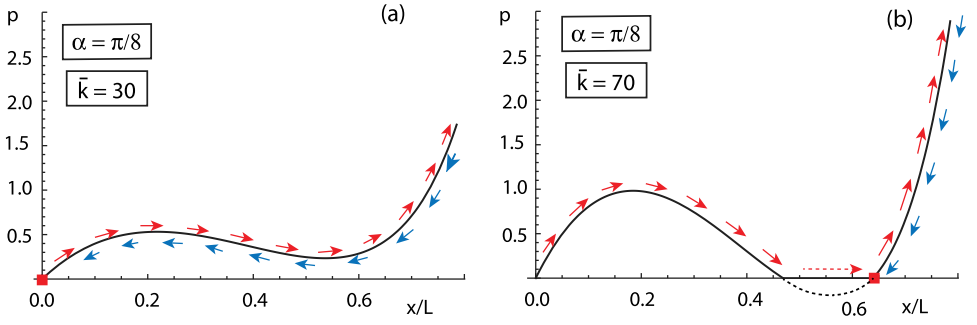

Fig. 8. Force–deflection behavior for two different spring ratios in terms of vertical position, measured from an initial rise of $\alpha = \pi/8$, (a) a return to the initial shape on load removal, (b) a system that remains in a snapped-state on load removal. (For interpretation of the references to color in this figure legend, the reader is referred to the web version of this article.)

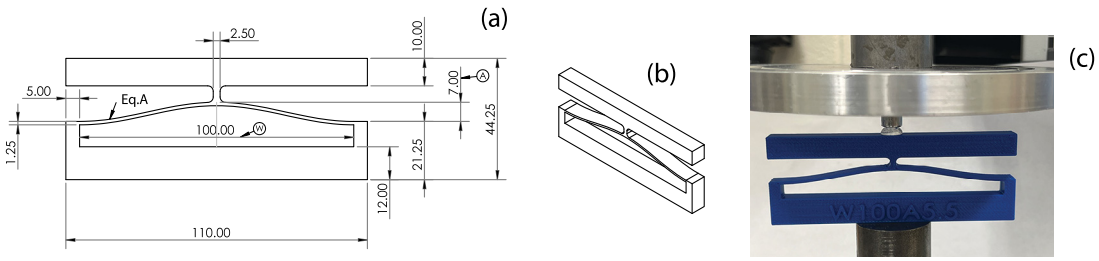

Fig. 9. A typical experimental element. (a) the dimensions (in mm) with the equation of the curved component given by $A/2(1-\cos(2\pi x/L))$, where A is the central rise (5.25–7.5 mm), and L is the span (100 mm), (b) an angled view, (c) a 3D-printed specimen in the loading machine.

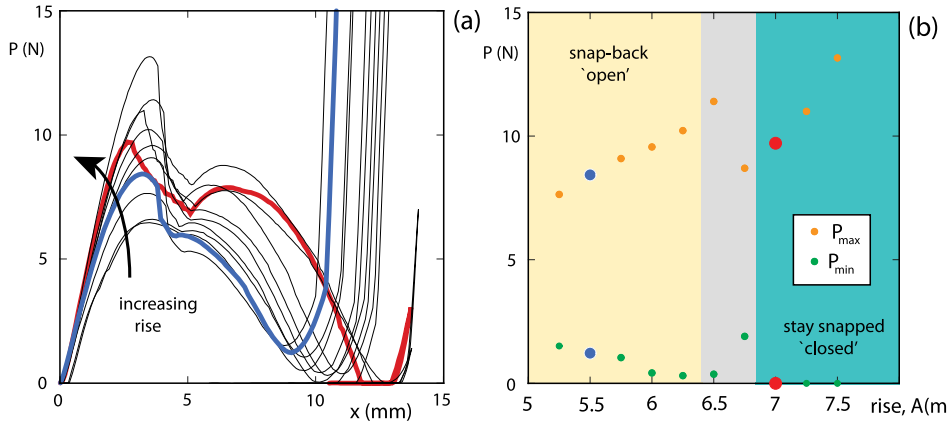

Fig. 10. Force–deflection relations for ten snapping elements, loading and unloading, (b) the loci of maximum and minimum loads. The behavior highlighted in red and blue are considered in more detail in Fig. 11. (For interpretation of the references to color in this figure legend, the reader is referred to the web version of this article.)

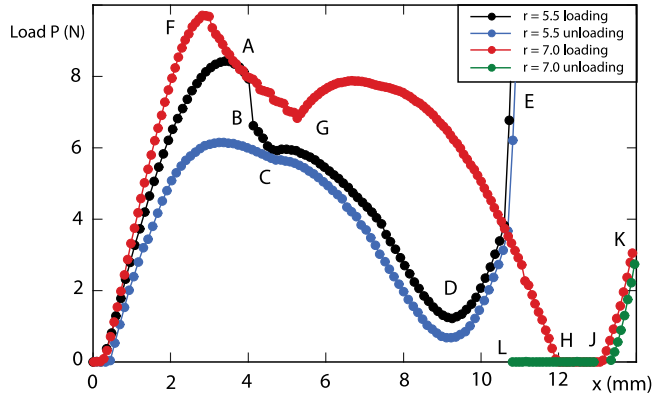

Fig. 11. Force–deflection behavior for two elements, one that snaps-back (black and blue) and one that stays in a snapped configuration (red and green). (For interpretation of the references to color in this figure legend, the reader is referred to the web version of this article.)

E). The direction of loading is reversed (the load cell moves up) and this path is indicated in blue data points. There appears to be a little hysteresis as a somewhat different path is followed during the return to the original shape.

For an arch with a slightly higher rise, for example 7 mm we obtain the data shown in red and green in Fig. 11. A higher initial load is reached, nearly 10 N, in which the arch more distinctly bifurcates into an asymmetric shape (point F). On subsequent displacement one end again comes into contact (point G) before the load drops to zero. At this point (H) contact is lost until the load cell catches back up with the arch (point J) and proceeds to take more load until the direction of displacement is reversed (point K) and the color coding switches from red to green. The important difference is that now, when the force drops back down to zero, contact is again lost (point J), and the element remains closed as the load continues to move up, with the test terminated at point L.

We see a broad correspondence between the model in Fig. 8 and the experimental data in Fig. 11. Some of the differences are examined in the next section.

5. Limitations of the discrete model and discussion

There are a number of ways in which the discrete link-model differs from the 3D-printed (continuous) elements. In terms of the analogy with the 3D-printed systems described earlier, a shortcoming of the discrete model is the restriction to symmetric behavior. It is well-established that unless an arch-like structure is very shallow, there is typically a non-trivial asymmetric component to the deflection especially in the vicinity of where snap-through occurs for force-controlled loading. Typically, the loaded-straight configuration represents a very high level of strain energy, and an arch finds it much more energetically expedient to pass around this energy hill-top by deflecting asymmetrically. However, the geometry of the unit cells within a lattice tends to reduce the asymmetrical behavior, and in the context of the current study we are primarily interested in whether the systems exhibits bi-stability, rather than how it might transition from one equilibrium to

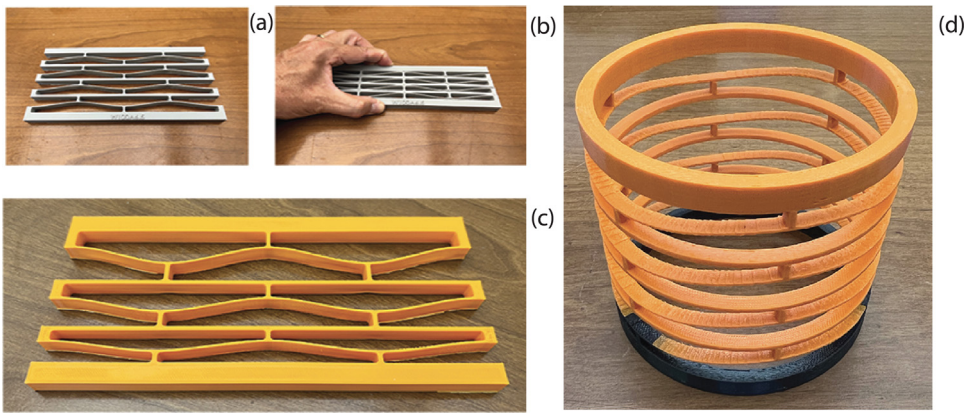

Fig. 12. Examples of 3D-printed lattices. (a) and (b) a simple lattice arrangement that exhibits snapping when compressed, but does not stay in the compressed configuration, (c) a degree of tailoring can be achieved by varying geometry, (d) a snapping lattice incorporated into a cylindrical arrangement.

another (with both free equilibrium shapes symmetric). It would be possible to measure the angle associated with this form of asymmetry, and even incorporate this effect into the discrete model.

Another issue, often important within a buckling context is the role of imperfections, where even very small deviations from a symmetric geometry (say) can have a profound effect on behavior under load [33]. The flat arch-like geometry is somewhat imperfection-sensitive (depending on the geometry) [33,54], and in referring to Fig. 3 it can be seen that a reasonable variation to this model might be to allow the two axial springs to have different stiffnesses, or having the lateral spring offset at a small angle from the vertical. The condition of one root transitioning into three roots is associated with a horizontal tangency, which *is* quite sensitive. This issue relates to the accuracy with which elements can be 3D-printed, especially in the thickness dimension, as well as certain limitations of common 3D-printer materials, e.g., a little plastic yielding, thermal effects, and stress concentrations. A small amount of viscoelasticity can also be observed in Fig. 10, in which some of the paths do not quite return to their original configuration when the load is removed. Also, in Fig. 11 an offset between the loading and unloading paths can be observed, and even a significantly different transition between symmetric and asymmetric behavior depending on the direction of loading. A slight discoloration was observed near the clamped ends of the flexible component, especially under repeated snapping, indicating some minor yielding of the material. This probably contributed to some of the subtle uncertainty in establishing an accurate transition point, i.e., the lightly-shaded region near a rise of 6.75 mm in Fig. 10(b).

6. Concluding remarks

This short note looks at a simple discrete structural model consisting of rigid links and elastic springs. The model was devised to shed light on the observed snapping behavior of some 3D-printed components, a classic example of buckling [55–57]. Under a typical sequence of loading (compressing and releasing), the system may snap-back to its original shape or remain in a post-snap configuration (bi-stability). The parameters of the model (representing geometry and stiffness) and their influence on this behavior is displayed. Specifically, the effect of the rise of the 3D-printed arches plays essentially the same role as the initial angle (α) of the theoretical model. Some 3D-printed elements were tested experimentally and data confirmed the transition to bi-stability.

Declaration of competing interest

The authors declare the following financial interests/personal relationships which may be considered as potential competing interests: Lawrence Virgin reports financial support was provided by National Science Foundation.

Data availability

Data will be made available on request.

Acknowledgments

The author is grateful for funding support from the NSF (CMMI 1926672). The opinions, findings, and conclusions, or recommendations expressed are those of the author(s) and do not necessarily reflect the views of the National Science Foundation. Thanks also, to Iman von Briesen, who 3D-printed some of the samples in the appendix as part of her undergraduate research project.

Appendix

Some examples of 3D-printed lattices were inspired by [3,4,40], and shown in Fig. 12.

These elements were printed with a variety of thicknesses, spans, and rises (with the flexible component in the form of a complete cosine wave). There is a broad analogy between these parameters and the springs and initial angles of the discrete model. 3D-printing the snapping elements in series or parallel suggests a versatile control over spring stiffness.

References

[1] Y. Zhang, Q. Wang, M. Tichem, F. van Keulen, Design and characterization of multi-stable mechanical metastructures with level and tilted stable configurations, Extreme Mech. Lett. 34 (2020) 100593, http://dx.doi.org/10.1016/j.eml.2019.100593.

[2] V. Sundararaman, M.P. O'Donnell, I.V. Chenchiah, P.M. Weaver, Toplogy morphing lattice structures, in: Conference on Smart Materials, Adaptive Structures and Intelligent Systems, ASME, 2021, http://dx.doi.org/10.1115/SMASIS2021-67531.

[3] T.R. Giri, R. Mailen, Controlled snapping sequence and energy absorption in multistable mechanical metamaterial cylinders, Int. J. Mech. Sci. 204 (2021) 106541, http://dx.doi.org/10.1016/j.ijmecsci.2021.106541.

[4] S. Shan, S.H. Kang, J.R. Raney, P. Wang, L. Fang, F. Candido, J.A. Lewis, K. Bertoldi, Multistable architected materials for trapping elastic strain energy, Adv. Mater. 27 (29) (2015) 4296–4301, http://dx.doi.org/10.1002/adma.201501708.

[5] L.N. Virgin, Y. Guan, R.H. Plaut, On the geometric conditions for multiple stable equilibria in clamped arches, Int. J. Nonlinear Mech. 92 (2017) 8–14, http://dx.doi.org/10.1016/j.ijnonlinmec.2017.03.009.

[6] Y. Zhao, A.J.J.M. Joseph, Z. Zhang, C. Ma, D. Gul, A. Schellenberg, N. Hu, Deterministic snap-through buckling and energy trapping in axially-loaded notched strips for compliant building blocks, Smart Mater. Struct. 29 (2020) http://dx.doi.org/10.1088/1361-665x/ab6486.

[7] D. Restrepo, N.D. Mankame, P.D. Zavattieri, Phase transforming cellular materials, Extreme Mech. Lett. 4 (2015) 52–60, http://dx.doi.org/10.1016/j.eml.2015.08.001, URL https://www.sciencedirect.com/science/article/pii/S2352431615000929.

[8] Y. Cao, M. Derakhshani, Y. Fang, G. Huang, C. Cao, Bistable structures for advanced functional systems, Adv. Funct. Mater. 31 (45) (2021) 2106231, http://dx.doi.org/10.1002/adfm.202106231.

[9] L. Rombouts, Dynamic bistable switches enhance robustness and accuracy of cell cycle transitions, PLoS Comput. Biol. 17 (1) (2021) 1–28, http://dx.doi.org/10.1371/journal.pcbi.1008231.

[10] T. Chen, O.R. Bilal, K. Shea, C. Daraio, Harnessing bistability for directional propulsion of soft, untethered robots, Proc. Natl. Acad. Sci. 115 (22) (2018) 5698–5702, http://dx.doi.org/10.1073/pnas.1800386115.

[11] Y. Chi, Y. Li, Y. Zhao, Y. Hong, Y. Tang, J. Yin, Bistable and multistable actuators for soft robots: Structures, materials, and functionalities, Adv. Mater. 34 (19) (2022) 2110384, http://dx.doi.org/10.1002/adma.202110384.

[12] Z. Ozdemir, E. Hernandez-Nava, A. Tyas, J.A. Warren, S.D. Fay, R. Goodall, I. Todd, H. Askes, Energy absorption in lattice structures in dynamics: Experiments, Int. J. Impact Eng. 89 (2016) 49–61, http://dx.doi.org/10.1016/j.ijimpeng.2015.10.007.

[13] I. Maskery, N.T. Aboulkhair, A.O. Aremu, C.J. Tuck, I.A. Ashcroft, Compressive failure modes and energy absorption in additively manufactured double gyroid lattices, Addit. Manuf. 16 (2017) 24–29, http://dx.doi.org/10.1016/j.addma.2017.04.003.

[14] O.A. Ganilova, J.J. Low, Application of smart honeycomb structures for automotive passive safety, Proc. Inst. Mech. Eng. D 232 (6) (2018) 797–811, http://dx.doi.org/10.1177/0954407017708916.

[15] N. Jin, F. Wang, Y. Wang, B. Zhang, H. Cheng, H. Zhang, Failure and energy absorption characteristics of four lattice structures under dynamic loading, Mater. Des. 169 (2019) 107655, http://dx.doi.org/10.1016/j.matdes.2019.107655.

[16] A. Montalbano, G.M. Fadel, G. Li, Design for energy absorption using snap-through bistable metamaterials, Mech. Based Des. Struct. Mach. (2021) 1–19, http://dx.doi.org/10.1080/15397734.2020.1867167.

[17] J.J. Andrew, J. Schneider, J. Ubaid, R. Velmurugan, N.K. Gupta, S. Kumar, Energy absorption characteristics of additively manufactured plate-lattices under low-velocity impact loading, Int. J. Impact Eng. 149 (2021) 103768, http://dx.doi.org/10.1016/j.ijimpeng.2020.103768.

[18] B.S. Yeow, C.J. Cai, M.S. Kalairaj, F.W. Hoo, Z.X. Lee, J.C.S. Tan, J.R. Ho, V.M. Ma, H. Huang, H. Ren, Origami-inspired snap-through bistability in parallel and curved mechanisms through the inflection of degree four vertexes, in: 2021 IEEE International Conference on Robotics and Automation, ICRA, 2021, pp. 10863–10869, http://dx.doi.org/10.1109/ICRA48506.2021.9562094.

[19] S.P. Pellegrini, N. Tolou, M. Schenk, J.L. Herder, Bistable vibration energy harvesters: A review, J. Intell. Mater. Syst. Struct. 24 (11) (2013) 1303–1312, http://dx.doi.org/10.1177/1045389X12444940.

[20] Y. Xia, M. Ruzzene, A. Erturk, Dramatic bandwidth enhancement in nonlinear metastructures via bistable attachments, Appl. Phys. Lett. 114 (9) (2019) 093501, http://dx.doi.org/10.1063/1.5066329.

[21] W. Nan, H. Yuncheng, F. Jiyang, Bistable energy harvester using easy snap-through performance to increase output power, Energy 226 (2021) 120414, http://dx.doi.org/10.1016/j.energy.2021.120414.

[22] B. Liu, C. Levi, S.F. Estdefen, Z. Wu, M. Duan, Evaluation of the double snap-through mechanism on the wave energy converter's performance, J. Marine. Sci. Appl. 20 (2021) 268–283, http://dx.doi.org/10.1007/s11804-021-00202-5.

[23] M.J. Frazier, D.M. Kochmann, Band gap transmission in periodic bistable mechanical systems, J. Sound Vib. 388 (2017) 315–326, http://dx.doi.org/10.1016/j.jsv.2016.10.041.

[24] E. Liu, X. Fang, J. Wen, Harmonic and shock wave propagation in bistable periodic structure: Regularity, randomness, and tunability, J. Vib. Control (2021) 10775463211031060, http://dx.doi.org/10.1177/10775463211031060.

[25] B. Deng, J.R. Raney, K. Bertoldi, V. Tournat, Nonlinear waves in flexible mechanical metamaterials, J. Appl. Phys. 130 (4) (2021) 040901, http://dx.doi.org/10.1063/5.0050271.

[26] T. Chen, J. Mueller, K. Shea, Integrated design and simulation of tunable, multi-state structures fabricated monolithically with multi-material 3D printing, Sci. Rep. 7 (2017) 45671, http://dx.doi.org/10.1038/srep45671.

[27] J. Bunyan, S. Tawfick, Exploiting structural instability to design architected materials having essentially nonlinear stiffness, Adv. Eng. Mater. 21 (2) (2019) 1800791, http://dx.doi.org/10.1002/adem.201800791.

[28] E.G. Loukaides, R.W.C. Lewis, C.R. Bowen, Additive manufacture of multistable structures, Smart Mater. Struct. 28 (2) (2019) 02LT02, http://dx.doi.org/10.1088/1361-665x/aae4f6.

[29] J.-S. Chen, H.-W. Tsao, Static snapping load of a hinged extensible elastica, Appl. Math. Model. 37 (18) (2013) 8401–8408, http://dx.doi.org/10.1016/j.apm.2013.03.040.

[30] K. Che, C. Yuan, J. Wu, H. Jerry Qi, J. Meaud, Three-Dimensional-Printed Multistable Mechanical Metamaterials With a Deterministic Deformation Sequence, J. Appl. Mech. 84 (1) (2016) http://dx.doi.org/10.1115/1.4034706.

[31] M. Vangbo, An analytical analysis of a compressed bistable buckled beam, Sensors Actuators A 69 (3) (1998) 212–216, http://dx.doi.org/10.1016/S0924-4247(98)00097-1.

[32] P.S. Harvey, L.N. Virgin, Coexisting equilibria and stability of a shallow arch: Unilateral displacement-control experiments and theory, Int. J. Solids Struct. 54 (2015) 1–11, http://dx.doi.org/10.1016/j.ijsolstr.2014.11.016.

[33] L.N. Virgin, Vibration of Axially-Loaded Structures, Cambridge University Press, 2007.

[34] M. Taffetani, X. Jiang, D.P. Holmes, D. Vella, Static bistability of spherical caps, Proc. R. Soc. Lond. Ser. A Math. Phys. Eng. Sci. 474 (2018) http://dx.doi.org/10.1098/rspa.2017.0910.

[35] K.R. Olympio, F. Gandhi, Zero Poisson's ratio cellular honeycombs for flex skins undergoing one-dimensional morphing, J. Intell. Mater. Syst. Struct. 21 (2010) http://dx.doi.org/10.1177/1045389X09355664.

[36] R. Lakes, Advances in negative Poisson's ratio materials, Adv. Mater. 5 (4) (1993) 293–296, http://dx.doi.org/10.1002/adma.19930050416.

[37] C. Huang, L. Chen, Negative Poisson's ratio in modern functional materials, Adv. Mater. 28 (37) (2016) 8079–8096, http://dx.doi.org/10.1002/adma.201601363.

[38] Z. Dong, Y. Li, T. Zhao, W. Wu, D. Xiao, J. Liang, Experimental and numerical studies on the compressive mechanical properties of the metallic auxetic reentrant honeycomb, Mater. Des. 182 (2019) 108036, http://dx.doi.org/10.1016/j.matdes.2019.108036.

[39] A. Rafsanjani, A. Akbarzadeh, D. Pasini, Snapping mechanical metamaterials under tension, Adv. Mater. 27 (39) (2015) 5931–5935, http://dx.doi.org/10.1002/adma.201502809.

[40] S. Sun, N. An, G. Wang, M. Li, J. Zhou, Snap-back induced hysteresis in an elastic mechanical metamaterial under tension, Appl. Phys. Lett. 115 (9) (2019) 091901, http://dx.doi.org/10.1063/1.5119275.

[41] S.N. Khaderi, V.S. Deshpande, N.A. Fleck, The stiffness and strength of the gyroid lattice, Int. J. Solids Struct. 51 (23) (2014) 3866–3877, http://dx.doi.org/10.1016/j.ijsolstr.2014.06.024.

[42] C. Ling, A. Cernicchi, M.D. Gilchrist, P. Cardiff, Mechanical behaviour of additively-manufactured polymeric octet-truss lattice structures under quasi-static and dynamic compressive loading, Mater. Des. 162 (2019) 106–118, http://dx.doi.org/10.1016/j.matdes.2018.11.035.

[43] Y. Wang, X. Ren, Z. Chen, Y. Jiang, X. Cao, S. Fang, T. Zhao, Y. Li, D. Fang, Numerical and experimental studies on compressive behavior of gyroid lattice cylindrical shells, Mater. Des. 186 (2020) 108340, http://dx.doi.org/10.1016/j.matdes.2019.108340.

[44] S. Li, M. Hu, L. Xiao, W. Song, Compressive properties and collapse behavior of additively-manufactured layered-hybrid lattice structures under static and dynamic loadings, Thin-Walled Struct. 157 (2020) 107153, http://dx.doi.org/10.1016/j.tws.2020.107153.

[45] C. Völlmecke, M. Todt, S. Yiatros, Buckling and postbuckling of architectured materials: A review of methods for lattice structures and metal foams, Composites and Advanced Materials 30 (2021) 26349833211003904, http://dx.doi.org/10.1177/26349833211003904.

[46] S.O. Obadimu, K.I. Kourousis, Additively manufactured lattice structures: A review, Aerospace 8 (2021) 207, http://dx.doi.org/10.3390/aerospace8080207.

[47] L.N. Virgin, R. Wiebe, S.M. Spottswood, T.G. Eason, Sensitivity in the structural behavior of shallow arches', Int. J. Nonlinear Mech. 58 (2014) 212–221, http://dx.doi.org/10.1016/j.ijnonlinmec.2013.10.003.

[48] J. Qiu, J.H. Lang, A.H. Slocum, A curved-beam bistable mechanism, J. Microelectromech. Syst. 13 (2) (2004) 137–146, http://dx.doi.org/10.1109/JMEMS.2004.825308.

[49] Y. Guan, L.N. Virgin, A pyramidal lattice frame: Pathways to inversion, Int. J. Struct. Stab. Dyn. 21 (2150020) (2021) http://dx.doi.org/10.1142/S0219455421500206.

[50] M.G. Tarantino, K. Danas, Programmable higher-order Euler buckling modes in hierarchical beams, Int. J. Solids Struct. 167 (2019) 170–183, http://dx.doi.org/10.1016/j.ijsolstr.2019.03.009.

[51] L.N. Virgin, Simultaneous buckling, contact, and load-carrying capacity, J. Eng. Mech. 147 (5) (2021) 04021023, http://dx.doi.org/10.1061/(ASCE)EM.1943-7889.0001926.

[52] J.G.A. Croll, A.C. Walker, Elements of Structural Stability, John Wiley and Sons, 1972.

[53] P. Bellini, The concept of snap-buckling illustrated by a simple model, Int. J. Nonlinear Mech. 7 (1972) http://dx.doi.org/10.1142/S0219455421500206.

[54] L.N. Virgin, Parametric studies of the dynamic evolution through a fold, J. Sound Vib. 110 (1) (1986) 99–109, http://dx.doi.org/10.1016/S0022-460X(86)80077-3.

[55] S.P. Timoshenko, J. Gere, Theory of Elastic Stability, Dover, 1961.

[56] L. Kollar, Structural Stability in Engineering Practice, E and FN Spon, 1999.

[57] G.H. Simitses, D.H. Hodges, Fundamentals of Structural Stability, Elsevier, 2006.